Journal of Energy Chemistry 25 (2016) 381–386

Contents lists available at ScienceDirect

Journal of Energy Chemistry

journal homepage: www.elsevier.com/locate/jechem

http://www.journals.elsevier.com/journal-of-energy-chemistry/

p-Type $CaFe_2O_4$ semiconductor nanorods controllably synthesized by molten salt method

Xin Liu[a,1], Junzhe Jiang[a,1], Yushuai Jia[a], Ailing Jin[a], Xiangshu Chen[a,*], Fei Zhang[a], Hongxian Han[b,*]

[a] Jiangxi Inorganic Membrane Materials Engineering Research Centre, College of Chemistry and Chemical Engineering, Jiangxi Normal University, Nanchang 330022, Jiangxi, China

[b] State Key Laboratory of Catalysis, Dalian Institute of Chemical Physics, Chinese Academy of Sciences, Dalian National Laboratory for Clean Energy, Dalian 116023, Liaoning, China

ARTICLE INFO

Article history:
Received 15 December 2015
Revised 29 December 2015
Accepted 18 January 2016
Available online 24 March 2016

Keywords:
p-Type semiconductor
$CaFe_2O_4$ nanorods
Molten salt
Crystal plane
Visible-light absorption

ABSTRACT

Pure phase, regular shape and well crystallized nanorods of p-type semiconductor $CaFe_2O_4$ have been fabricated for the first time by a facile molten salt assisted method, as confirmed by XRD, TEM, SEM and HRTEM. UV–vis diffuse reflectance spectra and Mott–Schottky plots show that the band structure of the $CaFe_2O_4$ nanorods is narrower than that of the $CaFe_2O_4$ nanoparticles synthesized by conventional method. The enhancement of the visible-light absorption is due to narrowness of the band gap in $CaFe_2O_4$ nanorods. The appropriate ratio between the molten salt and the $CaFe_2O_4$ precursors plays an important role in inhibiting the growth of the crystals along the (201) plane to give the desired nanorod morphology. This work not only demonstrates that highly pure p-type $CaFe_2O_4$ semiconductor with tunable band structure and morphology could be obtained using the molten salt strategy, but also affirms that the bandgap of a semiconductor may be tunable by monitoring the growth of a particular crystal plane. Furthermore, the facile eutectic molten salt method developed in this work may be further extended to fabricate some other semiconductor nanomaterials with a diversity of morphologies.

1. Introduction

Efficient separation of photogenerated charges serves as the driving force for the photocatalytic reactions, which is crucial for achieving high photocatalytic activity [1]. Fabrication of p–n junction photocatalysts is one of the ideal approaches to separate photogenerated charges [2,3]. Unfortunately, though various kinds of n-type semiconductors have been well studied, p-type semiconductors are still rare in study, nevertheless to say fabrication of efficient p–n junction photocatalysts. In order to develop p–n junction photocatalysts, it is necessary to develop and study p-type semiconductors [4].

$CaFe_2O_4$ is a p-type semiconductor (with band gap ~2.0 eV) composed of earth-abundant elements. Because it is inexpensive and environmentally friendly, $CaFe_2O_4$ has been widely investigated for various applications, such as pigments [5], absorbent of hydrogen sulfide for hot-gas cleaning [6], heterogeneous catalyst [7,8], photocatalyst for CO_2 reduction and degradation of pollutants [9–13] as well as photocathode material for photoelectrochemical hydrogen production [14–18]. However, controllable synthesis of highly pure $CaFe_2O_4$ crystals with specific morphology has not been reported so far. It is well known that the nanomaterials with specific morphologies, such as nanowires [19], nanorods [20] and nanobelts [21], may give remarkably different physical and chemical properties compared to the corresponding nanoparticle counterparts [22,23]. Tailor control of the morphology may render exposure of high-reactive crystal facets [24–26], well-aligned nano-architecture to provide short or fast pathway for transfer of charge carriers at a particular directions [27–30], and efficient inhibitation of photogenerated charge recombination to lead to enhanced photocatalytic and photovoltaic performances [31–33].

The morphology control of calcium ferrite-type compounds still remains a great challenge. For the preparation of $CaFe_2O_4$ without regular shape, solid-state reaction and polymerizable complex are the two commonly used methods [13,34–37]. However, to the best of our knowledge, there have been no reports on the controllable synthesis of $CaFe_2O_4$ nanomaterials with regular morphology. Here, we report for the first time that well defined $CaFe_2O_4$ nanorod crystals could be synthesized via a facile polymerizable

* Corresponding author. Tel: +86 411 84379760; Fax: +86 411 84694447.
** Corresponding author.
E-mail addresses: cxs66cn@jxnu.edu.cn (X. Chen), hxhan@dicp.ac.cn (H. Han).
[1] The authors contributed equally to this work.

http://dx.doi.org/10.1016/j.jechem.2016.03.019
2095-4956/

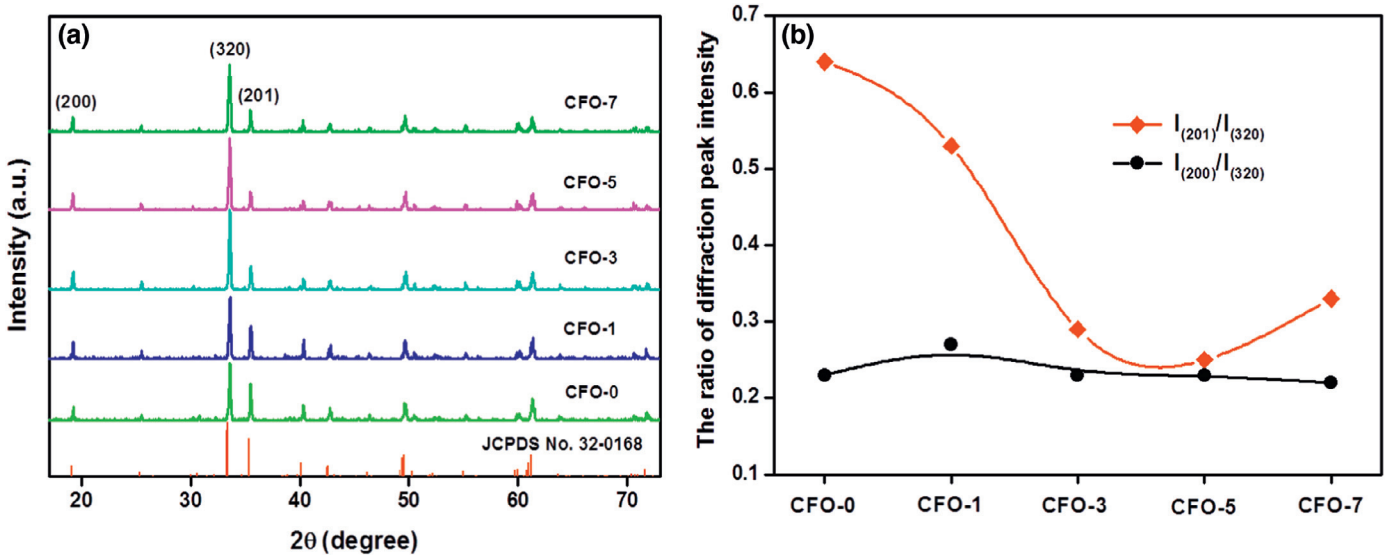

Fig. 1. (a) XRD patterns of $CaFe_2O_4$ samples synthesized with different amounts of molten salt, and (b) the relative intensity ratios of the diffraction peaks (201)/(320) and (200)/(320).

complex method in a eutectic mixture of NaCl and KCl molten salt. The introduction of the molten salt gives great benefit in nanorod morphology control by inhibiting the growth of the specific crystal plane.

2. Experimental

2.1. Preparation of the materials

$Fe(NO_3)_3{\cdot}9H_2O$ (98.5%) and $Ca(NO_3)_2{\cdot}4H_2O$ (99%) were purchased from Aladdin Industrial Corporation. Ethylene glycol (≥99.0%), citric acid (≥99.5%), NaCl (≥99.5%) and KCl (≥99.5%) were purchased from Sinopharm Chemical Reagent Co., Ltd. All of the reagents were used as received without further purification.

$CaFe_2O_4$ nanorods were prepared by polymerizable complex method in a molten salt of NaCl and KCl mixture. In a typical experiment, $Ca(NO_3)_2{\cdot}4H_2O$ (4.723 g) and $Fe(NO_3)_3{\cdot}9H_2O$ (16.160 g) were stirred and dissolved in deionized water (20 mL) containing citric acid (8.406 g) at room temperature, followed by addition of ethylene glycol (8 mL) to yield a transparent solution. The reaction mixture was dried at 80 °C for 12 h to evaporate water. Subsequent polyesterification at 130 °C for 12 h followed by pyrolysis at 350 °C for 2 h gave solid $CaFe_2O_4$ precursor, which was divided into several portions and blended with NaCl and KCl (molten salt) in the molar ratios of 1:0:0, 1:1:1, 1:3:3, 1:5:5 and 1:7:7. The thoroughly ground samples were then loaded into a high purity alumina crucibles and heated in air at 900°C for 5 h in a muffle furnace. After washed with boiling deionized water for several times to remove any residual salt, the products were dried in an oven at 80 °C overnight. The final products prepared as the above molar ratios of $CaFe_2O_4$ precursor to molten salt components are denoted as CFO-0, CFO-1, CFO-3, CFO-5 and CFO-7, respectively.

2.2. Characterization

X-ray diffraction (XRD) patterns were recorded on a Rigaku RINT-2200 diffractometer equipped with a Cu$K\alpha$ radiation source operating at a voltage of 40 kV and a current of 20 mA. The morphologies of the samples were examined by scanning electron microscopy (SEM) on a Hitachi SU-8020 cold field emission instrument. High-resolution transmission electron microscopy (HRTEM) images were taken on a JEOL JEM-2100 microscope at 200 kV. UV–vis diffuse reflectance spectra (UV–vis DRS) were recorded on a UV–vis spectrophotometer (JASCO V-750) equipped with an integrating $BaSO_4$ sphere. Thermogravimetry (TG) and derivative thermogravimetry (DTG) were carried out on a Diamond TG/DTA apparatus.

The Mott–Schottky plots were measured in a conventional three-electrode glass cell mode on an electrochemical workstation (CHI660A, Shanghai Chenhua Instruments, China). The thin films of the $CaFe_2O_4$ samples prepared by electrophoretic deposition method were used as the working electrodes. Pt plate and a saturated calomel electrode (SCE) were used as the counter electrode and the reference electrode, respectively. A 0.5 M Na_2SO_4 solution was used as the electrolyte.

3. Results and discussion

3.1. Crystal structure and morphology

Fig. 1(a) shows the XRD patterns of the synthesized $CaFe_2O_4$ samples. It can be seen that all of the samples exhibit diffraction peaks corresponding to the orthorhombic phase $CaFe_2O_4$ (JCPDS-32-0168). No observation of significant impurity peaks is an indication that the synthesized $CaFe_2O_4$ samples are in high quality. For comparison, the (320) peak was used as the internal standard to normalize all of the XRD patterns and the peak intensity ratios of (201)/(320) and (200)/(320) are plotted as shown in Fig. 1(b). No obvious changes in (200)/(320) intensity ratio are observed for all five samples, indicating that molten salt does not affect the growth of the $CaFe_2O_4$ on this direction. However, it is evident that the intensity ratio of (201)/(320) dramatically decreases with the increase of the molten salt. Increasing the amounts of the added molten salt during synthesis by decreasing the $CaFe_2O_4$ precursor/NaCl/KCl molar ratio from 1:0:0 to 1:7:7 results in the decrease of the (201)/(320) intensity ratio from 0.64 for CFO-0 to the minimum value of 0.25 for CFO-5. This strongly suggests that the growth of the $CaFe_2O_4$ crystals along the (201) plane is largely inhibited with the increase of the amount of the NaCl–KCl molten salt. Furthermore, such inhibitation of crystal growth towards a particular direction seems to have optimal conditions, as is evident from the trend that further increase in

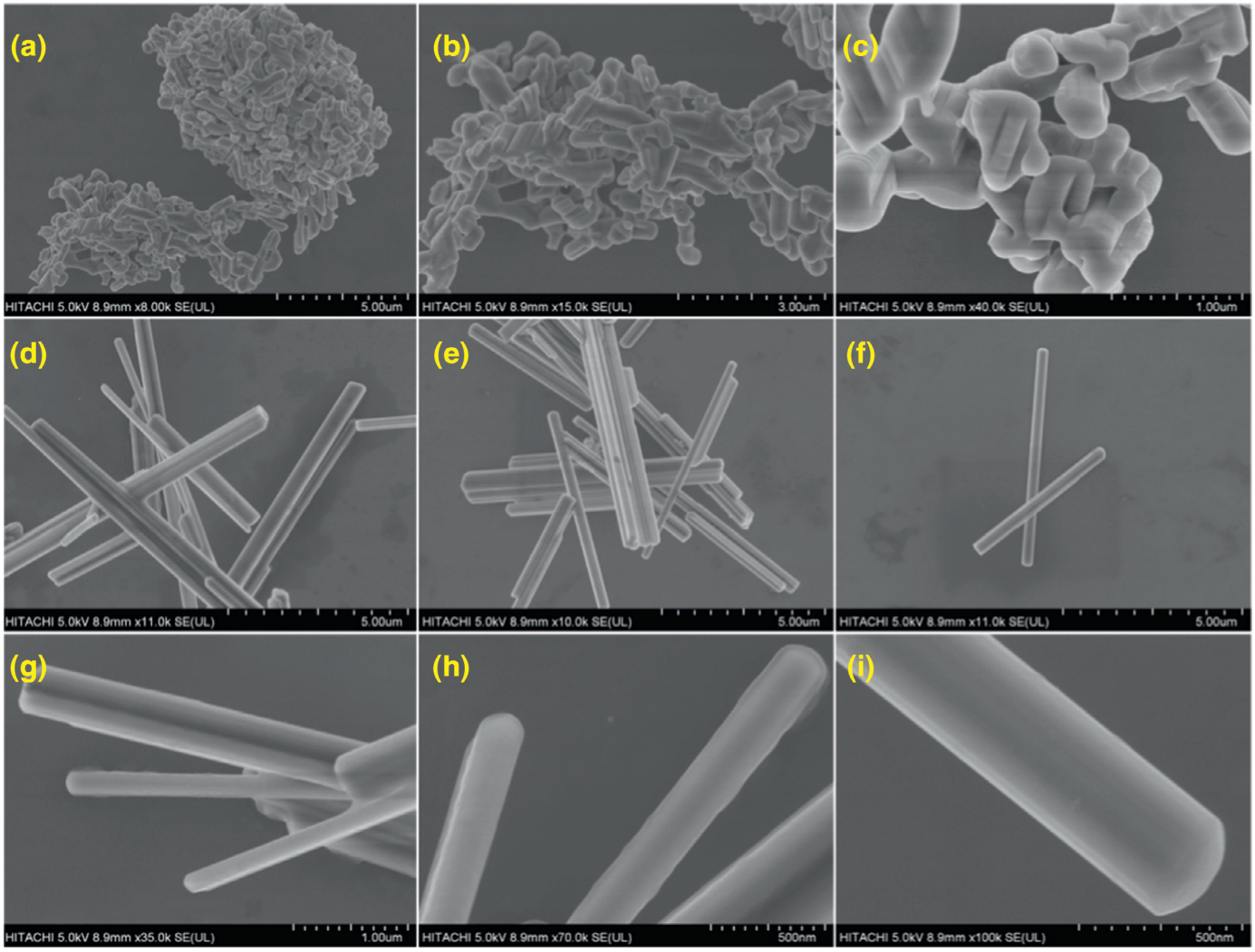

Fig. 2. SEM images of (a)–(c) CFO-0 $CaFe_2O_4$ particles prepared in the absence of molten salt, and (d)–(i) CFO-5 $CaFe_2O_4$ nanorods prepared in the presence of molten salt.

the amount of the molten salt leads to slight increase of the (201)/(320) peak intensity ratio to 0.33 for CFO-7.

Fig. 2 shows the typical SEM images of CFO-0 and CFO-5 samples. The irregularly shaped particles of CFO-0 can be observed in Fig. 2(a)–(c). Due to serious aggregation, the particle size of CFO-0 ranges from hundreds of nanometers to several micrometers. However, the CFO-5 sample synthesized in the presence of the molten salt exhibits significantly different morphologies. As shown in Fig. 2(d)–(g), CFO-5 shows nanorod-like structure with widths in the range of 200–500 nm and the lengths up to a few micrometers. And as shown in the typical SEM images of some representative single rods (Fig. 2h and i), most of the $CaFe_2O_4$ nanorods are very straight and uniform with smooth surfaces, although some of the nanorods are slightly agglomerated.

The microstructure and lattice parameters of the synthesized CFO-5 sample were further examined by TEM and HRTEM. The low magnification TEM images of the typical single $CaFe_2O_4$ nanorods (Fig. 3(a) and (b)) have smooth surfaces, which is in good accordance with the SEM results. The width of the nanorods is about 350 nm and 250 nm, respectively, which is also consistent with the observation by SEM in larger scales. The HRTEM image of the side surface of the $CaFe_2O_4$ nanorod (corresponding to the area marked with a yellow square in Fig. 3(b) is presented in Fig. 3(c). The average lattice spacing is well defined to be 0.27 nm, indicating that the side of the nanorod is the (320) plane of the orthorhombic $CaFe_2O_4$ single crystals.

3.2. Determination of the band structure

The UV–vis diffuse reflectance spectra (DRS) of CFO-0 and CFO-5 are shown in Fig. 4(a), and it can be seen that both of the samples show efficient visible light absorption. In order to determine the exact bandgap energies of the $CaFe_2O_4$ samples, extrapolation of the plots of the $(\alpha h\nu)^2$ vs. photon energy $(h\nu)$ was performed in Fig. 4(b), which was converted from DRS spectra based on the following formula [38,39]: $\alpha h\nu = A(h\nu E_g)^{n/2}$, where α, h, ν, A, and E_g are the absorption coefficient, Planck constant, light frequency, constant value and bandgap energy, respectively. The index n depends on the transition characteristic of a semiconductor, that is, direct transition ($n = 1$) or indirect transition ($n = 4$). The best fit of $(\alpha h\nu)^2$ vs. E_g is obtained only when n is 1, implying that the direct transition across the energy bandgap is allowed. So the bandgap energies of the synthesized $CaFe_2O_4$ materials are evaluated by the interception of the tangents to the X-axis. Thus, the bandgap energies of CFO-0 and CFO-5 were determined to be 1.89 eV and 1.82 eV, respectively.

The flat-band potentials (E_{fb}) of CFO-0 and CFO-5, which reflect the band positions of semiconductors, were determined by

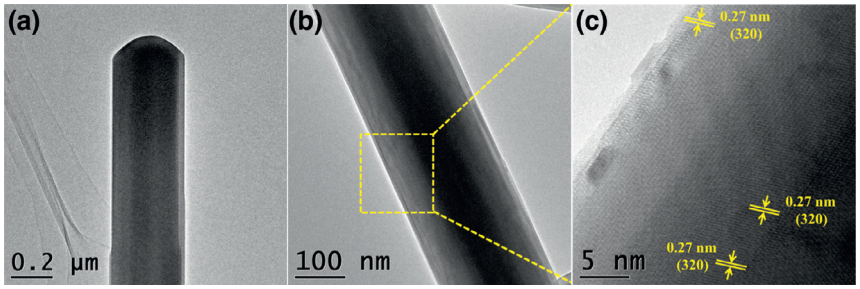

Fig. 3. TEM images (a) and (b), and HRTEM image (c) of CFO-5 $CaFe_2O_4$ nanorods.

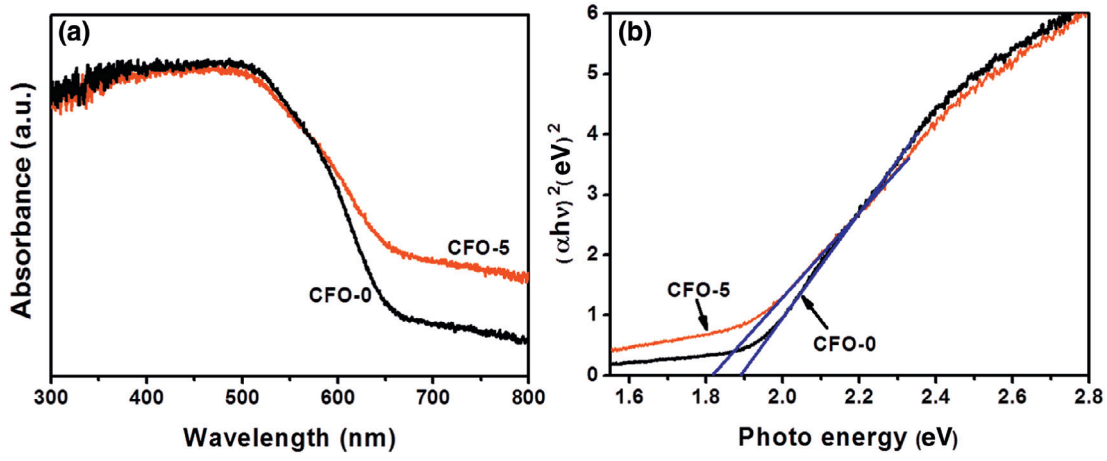

Fig. 4. (a) UV–vis diffuse reflectance spectra and (b) plots of the $(\alpha h\nu)^2$ *v*s. photon energy $(h\nu)$ of CFO-0 and CFO-5 samples.

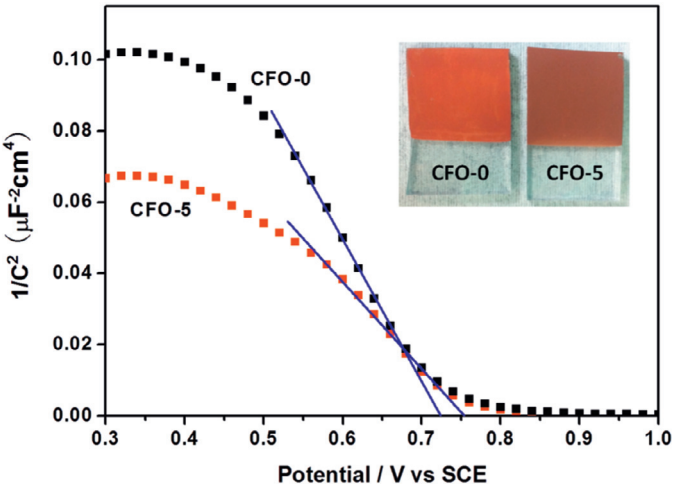

Fig. 5. Mott–Schottky plots of the CFO-0 and CFO-5 samples. Inset: the photograph of $CaFe_2O_4$ electrodes used for the electrochemical measurements.

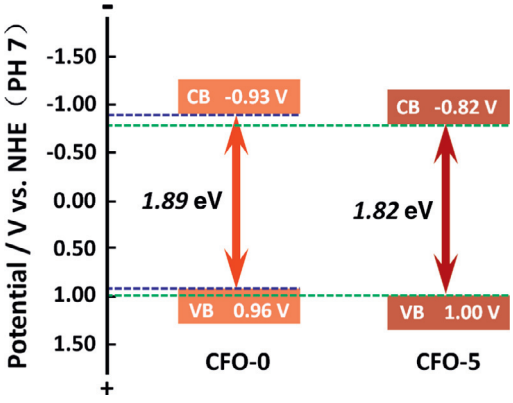

Fig. 6. Scheme of the band structures of CFO-0 and CFO-5 samples.

Mott–Schottky plots (Fig. 5) recorded in 0.5 M Na_2SO_4 solution. Both CFO-0 and CFO-5 show negative slopes in the Mott–Schottky plots, indicating p-type character of the materials [40]. The E_{fb} of CFO-0 and CFO-5 is obtained by the extrapolation of the Mott-Schottky plots of C^{-2} vs. E using the following equation: $1/C_{sc}^2 = 2(EE_{fb}\kappa T/e)/e\varepsilon\varepsilon_0 N_D$ [41], where C_{sc} is the space charge capacitance per unit surface area of the semiconductor, E is the applied potential, E_{fb} is the flat-band potential, κ is the Boltzmann constant, T is the temperature in Kelvin, e is the electronic charge unit, ε is the dielectric constant of the semiconductor layer, ε_0 is the permittivity of the vacuum, and N_D is the donor density. When $1/C^2$ is zero, the obtained X-intercept equals to E_{fb}. Thus the estimated E_{fb} of CFO-5 is ca. 0.76 V vs. SCE at pH 7, which is more positive than that of CFO-0 by ca. 0.04 V. For a p-type semiconductor, the E_{fb} lies very close to the top of the valance band VB) [42]. Therefore, the VBs are roughly estimated as the same as the flat-band potentials for easy comparison, i.e., the VBs of CFO-0 and CFO-5 are approximately 0.72 V and 0.76 V (vs. SCE at pH 7), respectively (The actual VBs should be slightly more negative than these values).

Hence, the entire band structure of the synthesized materials could be plotted as shown in Fig. 6. It can be seen that the bottom of conduction band (CB) and the top of VB lie around –0.93 and 0.96 V for CFO-0 and –0.82 and 1.00 V for CFO-5, respectively (all of the potentials are normalized to NHE, E (vs. NHE) = E (vs. SCE) + 0.24 V). Overall, the CFO-5 sample has slightly narrower bandgap compared to that of the CFO-0, which is beneficial for the visible light absorption. It should be noted that the CB of CFO-5 is

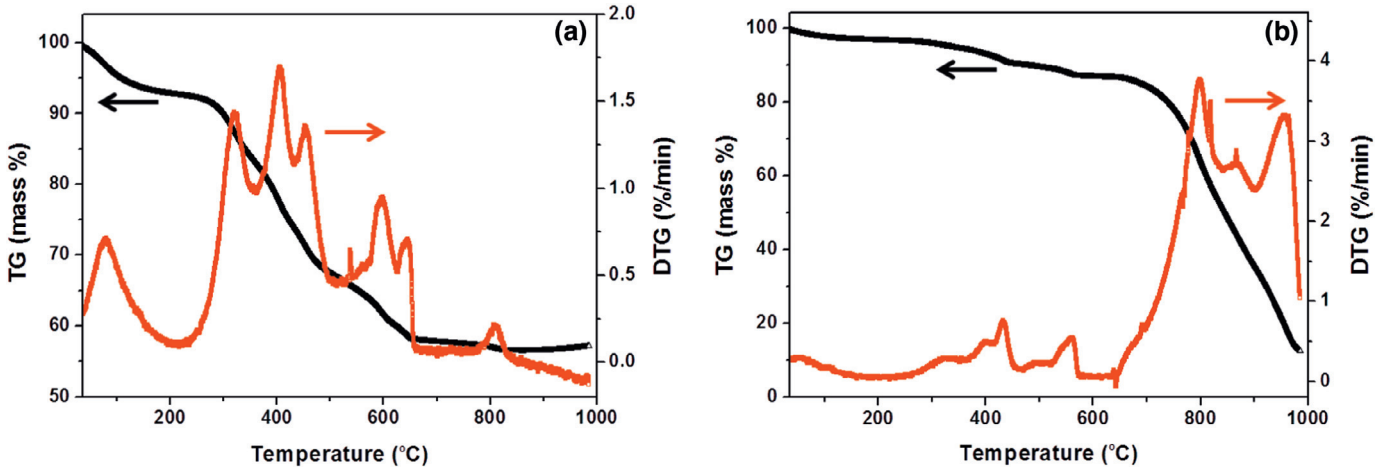

Fig. 7. TG/DTG curves of (a) pure $CaFe_2O_4$ precursors to CFO-0, and (b) the mixture of $CaFe_2O_4$ precursors and NaCl–KCl binary molten salt (1:5:5) to CFO-5.

ca. 0.11 V more positive than that of the CFO-0 but both of which values are negative enough to reduce proton; while the VB potential of CFO-5 is only ca. 0.04 V more positive than that of CFO-0, which means that both of the samples cannot oxidize water. The differences in band potential and band gap of CFO-0 and CFO-5 samples may be originated from the different exposure ratios of the (201) plane as shown in the previous section. Similar phenomenon was also reported by Yang et al., who suggested that the shift of CB potential of the rutile TiO_2 nanorods is largely due to the variation of the exposed facets [43].

3.3. The effect of the molten salt on the growth of the $CaFe_2O_4$ nanorods

To understand the effect of the molten salt on the growth mechanism of $CaFe_2O_4$ nanorods, TG/DTG analyses (Fig. 7) were carried out for the typical samples of CFO-0 and CFO-5. The thermal degradation of the pure $CaFe_2O_4$ precursors without molten salt occurs in three processes as indicated by the TG/DTG curves (Fig. 7(a)). The first process of weight loss (~5%) with maximum at ca. 78 °C is in the range of 50 °C to 150 °C, which corresponds to the release of adsorbed water molecules. The main weight loss (~30%) occurs in the second process between 250 °C and 500 °C with three peaks at 319 °C, 405 °C and 453 °C, which may be accountable for the decomposition of the polymeric chains. Further increase of the temperature results in the removal of the residual polymers and pyrolysis products, as indicated by the third weight loss of about 10% between 500 °C and 650 °C. The tiny weight loss above 650 °C was also observed, which might be due to further crystallization of the $CaFe_2O_4$ nanoparticles.

However, the TG/DTG curves of the $CaFe_2O_4$ precursors in the presence of NaCl–KCl molten salt to give CFO-5 (Fig. 7(b)) are quite different compared to those of the CFO-0. Though the DTG curve below 650 °C is similar to that of CFO-0 with the three weight loss processes which is an indication that the addition of molten salt does not change the basic processes in this temperature range, the overall weight loss below 650 °C is not as significant as that of CFO-0 (Fig. 7(a)) which might be due to presence of much less $CaFe_2O_4$ precursors. However, significant weight loss was observed when the temperature was increased to above 700 °C, as evidenced by the appearance of sharp DTG peaks between the temperature of 700 °C and 1000 °C. Considering that the melting point of eutectic salt medium of NaCl and KCl with a molar ratio of 1:1 is around 658 °C [44], the weight loss above 700 °C can be attributed to the gradual volatilization of NaCl and KCl [45]. The maximum rate of the weight loss is at ca. 800 °C as indicated by the DTG curve, while the center of the weight loss between 700 °C–1000°C is at ca. 900 °C, the exact temperature of which was applied for the crystallization of the $CaFe_2O_4$ nanorods.

The comparison of the overall DTG curves also indicates that the weight loss for the formation of CFO-5 mainly occurs at high temperature above 650 °C, while that for the formation of CFO-0 at temperature below 650 °C. The TG/DTG study also reveals that 900 °C is the optimal crystallization temperature for the synthesis of the $CaFe_2O_4$ nanorods. That is, accompanying with gradual melting and volatilization of NaCl and KCl, orthorhombic phase $CaFe_2O_4$ nanorods begin to grow and crystallize, and finally well-aged at temperature of 900 °C. Obviously, the molten salt of NaCl and KCl mixture plays an important role in the preparation of $CaFe_2O_4$ nanorods. Detailed mechanism for the formation of $CaFe_2O_4$ nanorods is not clear yet [44], but our primary experimental results give some meaningful clues. Firstly, the NaCl–KCl molten salt with low viscosity may provide a fluent liquid phase to improve the mobility of seed crystals during the nucleation and growth of nanorods [46]. Secondly, the Na^+, K^+ and Cl^- ions dissociated from the molten salt can be selectively adsorbed on the surface of $CaFe_2O_4$ seed crystals and thus change the energy of crystal surface [47], resulting in the formation of $CaFe_2O_4$ nanorods along the defined planes. The possible formation pathway of $CaFe_2O_4$ nanorods is illustrated in Fig. 8.

4. Conclusions

In this study, p-type semiconductor $CaFe_2O_4$ nanorods with a width of 200–500 nanometers and a length of a few micrometers are successfully synthesized using a NaCl–KCl binary eutectic molten salt. Compared to $CaFe_2O_4$ nanoparticles synthesized with conventional polymerized complex method, $CaFe_2O_4$ nanorods synthesized with molten salt method exhibit improved visible-light absorption capacity. It was proposed that the narrowness of the bandgap of the $CaFe_2O_4$ nanorods compared to the $CaFe_2O_4$ nanoparticles might be due to inhibiting the growth of the former along the (201) plane. In the meantime, a possible molten salt assisted mechanism for the growth of the $CaFe_2O_4$ nanorods is proposed based on the experimental results. This work not only demonstrates a new avenue for the controllable synthesis of nanorod shaped semiconductors, but also affirms that the bandgap of a semiconductor may be tunable by monitoring the growth of a particular crystal plane. Furthermore, the facile eutectic molten salt method developed in this work may be further extended to

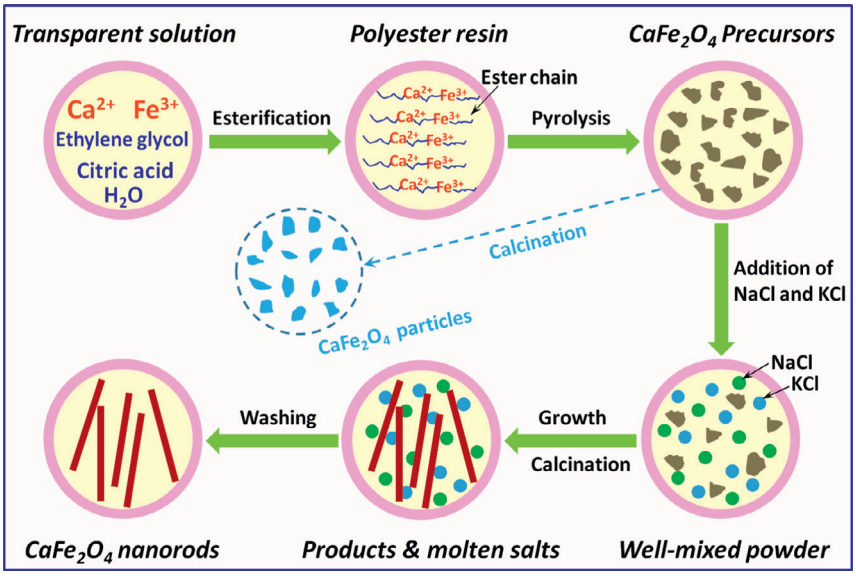

Fig. 8. Illustration of the synthesis and growth process of $CaFe_2O_4$ nanorods. The dashed arrow indicates the preparation process of $CaFe_2O_4$ particles in the absence of molten salt.

fabricate some other semiconductor nanomaterials with a diversity of morphologies. Photocatalytic H_2 production reactions by loading appropriate cocatalysts, as well as fabrication of p–n junction photocatalysts for overall water splitting with the synthesized $CaFe_2O_4$ nanorods are in the progress.

Acknowledgments

The authors gratefully acknowledge the supports from the National Natural Science Foundation of China (nos. 21473189 and 21503100), the 973 National Basic Research Program of China (no. 2014CB239401), and the Natural Science Foundation of Jiangxi Province of China (no. 20151BAB213010).

References

[1] J. Yang, D. Wang, H. Han, C. Li, Acc. Chem. Res. 46 (2013) 1900.
[2] F. Meng, J. Li, S.K. Cushing, M. Zhi, N. Wu, J. Am. Chem. Soc. 135 (2013) 10286.
[3] S. Ida, A. Takashiba, S. Koga, H. Hagiwara, T. Ishihara, J. Am. Chem. Soc. 136 (2014) 1872.
[4] Y. Jia, J. Yang, D. Zhao, H. Han, C. Li, J. Energy Chem. 23 (2014) 420.
[5] R.A. Candeia, M.I.B. Bernardi, E. Longo, I.M.G. Santos, A.G. Souza, Mater. Lett. 58 (2004) 569.
[6] N. Ikenaga, Y. Ohgaito, T. Suzuki, Energy Fuels 19 (2005) 170.
[7] F. Zhang, Z. Fang, Bioresour. Technol. 124 (2012) 440.
[8] B.-J. Xue, J. Luo, F. Zhang, Z. Fang, Energy 68 (2014) 584.
[9] Y. Matsumoto, M. Obata, J. Hombo, J. Phys. Chem. 98 (1994) 2950.
[10] Z. Zhang, W. Wang, Mater. Lett. 133 (2014) 212.
[11] C. Shifu, Z. Wei, L. Wei, Z. Huaye, Y. Xiaoling, C. Yinghao, J. Hazard. Mater. 172 (2009) 1415.
[12] S. Chen, W. Zhao, W. Liu, H. Zhang, X. Yu, Chem. Eng. J. 155 (2009) 466.
[13] H.G. Kim, P.H. Borse, J.S. Jang, E.D. Jeong, O.-S. Jung, Y.J. Suh, J.S. Lee, Chem. Commun. (2009) 5889.
[14] Y. Matsumoto, M. Omae, K. Sugiyama, E. Sato, J. Phys. Chem. 91 (1987) 577.
[15] S. Ida, K. Yamada, T. Matsunaga, H. Hagiwara, Y. Matsumoto, T. Ishihara, J. Am. Chem. Soc. 132 (2010) 17343.
[16] K. Sekizawa, T. Nonaka, T. Arai, T. Morikawa, ACS Appl. Mater. Interfaces 6 (2014) 10969.
[17] J. Cao, T. Kako, P. Li, S. Ouyang, J. Ye, Electrochem. Commun. 13 (2011) 275.
[18] S. Ida, K. Yamada, T. Matsunaga, H. Hagiwara, T. Ishihara, T. Taniguchi, M. Koinuma, Y. Matsumoto, Electrochemistry 79 (2011) 797.
[19] Y. Wu, Y. Cui, L. Huynh, C.J. Barrelet, D.C. Bell, C.M. Lieber, Nano Lett. 4 (2004) 433.
[20] B. Cheng, J.M. Russell, W.S. Shi, L. Zhang, E.T. Samulski, J. Am. Chem. Soc. 126 (2004) 5972.
[21] Z.W. Pan, Z.R. Dai, Z.L. Wang, Science 291 (2001) 1947.
[22] Y.N. Xia, P.D. Yang, Y.G. Sun, Y.Y. Wu, B. Mayers, B. Gates, Y.D. Yin, F. Kim, Y.Q. Yan, Adv. Mater. 15 (2003) 353.
[23] M.-A. Einarsrud, T. Grande, Chem. Soc. Rev. 43 (2014) 2187.
[24] C.Z. Wen, H.B. Jiang, S.Z. Qiao, H.G. Yang, G.Q. Lu, J. Mater. Chem. 21 (2011) 7052.
[25] H. Xu, P. Reunchan, S. Ouyang, H. Tong, N. Umezawa, T. Kako, J. Ye, Chem. Mater. 25 (2013) 405.
[26] E. Grabowska, M. Diak, M. Marchelek, A. Zaleska, Appl. Catal. B Environ. 156 (2014) 213.
[27] Y. Rui, Y. Li, Q. Zhang, H. Wang, CrystEngComm 15 (2013) 1651.
[28] M. Wang, C. Xing, K. Cao, L. Zhang, J. Liu, L. Meng, J. Mater. Chem. A 2 (2014) 9496.
[29] X. Fan, H. Zhang, N. Du, P. Wu, X. Xu, Y. Li, D. Yang, Nanoscale 4 (2012) 5343.
[30] B. Lee, P. Guo, S.-Q. Li, D.B. Buchholz, R.P.H. Chang, ACS Appl. Mater. Interfaces 6 (2014) 17713.
[31] H.J. Yun, H. Lee, J.B. Joo, W. Kim, J. Yi, J. Phys. Chem. C 113 (2009) 3050.
[32] A. Salant, M. Shalom, Z. Tachan, S. Buhbut, A. Zaban, U. Banin, Nano Lett. 12 (2012) 2095.
[33] M. Guo, P. Diao, X.D. Wang, S.M. Cai, J. Solid State Chem. 178 (2005) 3210.
[34] N. Sharma, K.M. Shaju, G.V.S. Rao, B.V.R. Chowdari, J. Power Sources 124 (2003) 204.
[35] J. Yin, X. Lv, S. Xiang, C. Bai, B. Yu, ISIJ Int. 53 (2013) 1571.
[36] L.J. Berchmans, M. Myndyk, K.L. Da Silva, A. Feldhoff, J. Subrt, P. Heitjans, K.D. Becker, V. Sepelak, J. Alloys Compd. 500 (2010) 68.
[37] L. Khanna, N.K. Verma, Mater. Sci. Semicond. Process. 16 (2013) 1842.
[38] N. Serpone, D. Lawless, R. Khairutdinov, J. Phys. Chem. 99 (1995) 16646.
[39] Y. Jia, S. Shen, D. Wang, X. Wang, J. Shi, F. Zhang, H. Han, C. Li, J. Mater. Chem. A 1 (2013) 7905.
[40] K.-S. Ahn, T. Deutsch, Y. Yan, C.-S. Jiang, C.L. Perkins, J. Turner, M. Al-Jassim, J. Appl. Phys. 102 (2007) 023517.
[41] S.N. Frank, A.J. Bard, J. Am. Chem. Soc. 97 (1975) 7427.
[42] S.R. Morrison, Electrochemistry at Semiconductor and Oxidized Metal Electrodes, Plenum Press, New York, 1980 (chapter 4).
[43] Z. Yang, B. Wang, J. Zhang, H. Cui, Y. Pan, H. An, J. Zhai, Phys. Chem. Chem. Phys. 17 (2015) 18670.
[44] X. Liu, N. Fechler, M. Antonietti, Chem. Soc. Rev. 42 (2013) 8237.
[45] S. Osada, D. Kuchar, H. Matsuda, J. Mater. Cycles Waste 11 (2009) 367.
[46] Z.W. Chen, J. Du, H.J. Zhang, Z. Jiao, M.H. Wu, C.H. Shek, C M.L. Wu, J.K.L. Lai, Acta Mater. 57 (2009) 4632.
[47] X. Ke, J. Cao, M. Zheng, Y. Chen, J. Liu, G. Ji, Mater. Lett. 61 (2007) 3901.